

1,2-propanediol ameliorated radiation-induced intestinal injury in mice

Received: 7 October 2025

Accepted: 5 March 2026

Published online: 11 March 2026

Cite this article as: Zhao J., Zhao C., Shen X. *et al.* 1,2-propanediol ameliorated radiation-induced intestinal injury in mice. *Sci Rep* (2026). <https://doi.org/10.1038/s41598-026-43614-5>

Jiwei Zhao, Chunan Zhao, Xing Shen, Ying Jiang, Xun Wang, Aoqiang Ji, Xuewen Zhang, Shuang Xing, Gang Sun, He Xiao & Zuyin Yu

We are providing an unedited version of this manuscript to give early access to its findings. Before final publication, the manuscript will undergo further editing. Please note there may be errors present which affect the content, and all legal disclaimers apply.

If this paper is publishing under a Transparent Peer Review model then Peer Review reports will publish with the final article.

ARTICLE IN PRESS

1,2-propanediol ameliorated radiation-induced intestinal injury in mice

Author: Jiwei Zhao^{#1,2}, Chunan Zhao^{#1}, Xing Shen^{#1}, Ying Jiang¹, Xun Wang¹, Aoqiang Ji¹, Xuwen Zhang¹, Shuang Xing¹, Gang Sun², He Xiao³, Zuyin Yu¹.

¹ Beijing Institute of Radiation Medicine, Beijing 100850, China

² Department of Gastroenterology and Hepatology, First Medical Center, Chinese PLA General Hospital, Beijing 100583, China

³ Beijing Institute of Pharmacology and Toxicology, Beijing 100850, China.

Those authors contributed equally#: Jiwei Zhao, Chunan Zhao, Xing Shen.

Corresponding authors:

Prof. Zuyin Yu, PhD, Beijing Institute of Radiation Medicine, Beijing 100850, China.

Email: yuzy79@163.com

Dr. Gang Sun, PhD, First Medical Center, Chinese PLA General Hospital, Beijing 100850, China

Email: sunok301@126.com

Prof. He Xiao, PhD, Beijing Institute of Pharmacology and Toxicology, Beijing 100850, China.

Email: crocodilexiao@sina.com

ARTICLE IN PRESS

Abstract

Radiotherapy is constricted by collateral normal tissue injury during treatment, particularly the gastrointestinal tracts, which is usually referred as radiation-induced gastrointestinal syndrome (RIGS). Currently, there is no FDA-approved agent for the prevention or treatment of RIGS. By using a mice model of RIGS, we demonstrated that 1,2-propanediol (1,2-PD) prevents radiation-induced fatal intestinal injury and significantly increases mice survival following lethal doses of radiation. 1,2-PD pretreatment also enhanced the survival of Lgr5⁺ISCs and improved crypts regeneration after radiation. Moreover, we confirmed 1,2-PD induces dormant cell cycle arrest in enterocytes and ameliorates DNA damage both in vitro and in vivo. Although we did have observed 1,2-PD pretreatment inhibiting P53-PUMA signal pathway, but fail to prove its relation with radiation resistance. In RNA sequencing, we have observed 1,2-PD pretreatment significantly upregulates the Hif-2 α , Hif-3 α and PPAR α target gene ACOX2, whilst downregulating the cell cycle drivers E2f3 and Cyclin D2. These results demonstrate that ISCs play a key role in radiation-induced intestinal regeneration and that 1,2-PD acts as a potent intestinal radioprotector.

Introduction

Radiotherapy is a crucial treatment modality for abdominal tumors, often delivered in combination with chemotherapy. However, the intensity of radiotherapy is limited by the tolerance of surrounding normal tissues, which features by vomiting, diarrhea, dehydration, sepsis, and intestinal bleeding[1]. Since more than 10 Gy irradiation exposure could primarily cause radiation-induced gastrointestinal syndrome (RIGS), the underlying mechanism of its overt vulnerability resides in the fast renewal of human intestinal epithelium. Furthermore, in treatment of certain pelvic and abdominal malignancies, RIGS has presented as main complications after radiation, and even limited full-term treatment[2].

Intestinal stem cells (ISCs) drive the physiological self-renewal and regenerative repair of damaged intestinal epithelia. Prevailing models assume that ISCs are made up of actively cycling crypt base columnar cells (CBCs) intermingled with Paneth cells, as well as much quiescent +4 cells positioned slightly above.[3, 4]. CBCs predominantly express Lgr5 and Olfm4 while +4 cells preferentially express Bmi1 and Hopx[3, 5-7]. However, ISCs subpopulations overlap in terms of surface markers expression and could interconvert in response to injury[4, 8, 9]. Convincing evidence indicate that Lgr5+ ISCs are dispensable for normal intestinal homeostasis[10], but loss of Lgr5+ ISCs profoundly impairs intestinal regeneration following radiation damage[11]. In this regard, improving the survival of Lgr5+ ISCs plays a key

role in intestinal radioprotection.

Ionizing radiations (IR) can induce single- and double-strand breaks (DSBs) causing genomic instability, and the extent of DNA damage determines the destiny of cell either completing DNA repair or ending in death program. Among ISCs, DNA damage is largely regulated by P53 pathway, and previous studies have demonstrated that P53 deficiency could lead to aggravated RIGS and mortality with exacerbated DNA damage in mice while the so-called "super p53" mice with an extra copy of p53 are more resistant to RIGS[2]. P53 modulates intestinal radiosensitivity by its downstream targets PUMA and P21[12, 13]. PUMA mediates radiation induced apoptosis in a P53-dependent manner and PUMA deficiency prevents apoptosis in ISCs and enhances crypt regeneration following high doses of radiation[14]. Hence, inhibition of P53-PUMA apoptotic pathway is proposed to be an effective therapeutic strategy in the treatment of RIGS.

1,2-Propanediol (1,2-PD) is a small molecule compound extensively used as a solvent or additive in pharmaceuticals, cell cryopreservation, cosmetics, electronic cigarettes, etc. 1,2-PD has been included by the FDA in the Guide to Inactive Components, with the injectable formulation that can be used at concentrations up to 80% in humans, and its intraperitoneal toxicity LD50=9720 mg/kg in mice[15]. In a recent study, 1,2-PD has been shown to have a clear radioprotective effect on the hematopoietic system in mice exposed to total body irradiation (TBI)[16]. In this study, we identified 1,2-PD

as a potent intestinal radiation protectant. Our findings indicated that 1,2-PD prophylactic administration strongly protects Lgr5+ ISCs and reduces DNA damage in crypt after radiation. And we demonstrated that 1,2-PD induces intestinal crypt cells into a reversible dormant proliferative state and confers intestinal radioprotection by influencing the P53-PUMA apoptosis pathways.

Results

1,2-PD ameliorates intestinal injury in mice after TBI.

To investigate the optimal administration timepoint and dose of 1,2-PD for intestinal radioprotection, 1,2-PD was intraperitoneally (i.p.) injected into RIGS mice model 12 h, 6 h, 3 h, 1 h before and 1 h after 15 Gy of irradiation. The BrdU immunohistochemistry (IHC) testing was performed 3.5 days after irradiation to detect the number of proliferating crypts. The results indicated that, comparing to the IR control group, the group treated with 1,2-PD 12 h, 6 h, 3 h, and 1 h before irradiation had more proliferating crypts 3.5 days after irradiation (Supplementary Fig. 1A and 1B). The optimal radioprotection effect was achieved in mice with 1,2-PD applied 3 h before irradiation. In contrast, no obvious increase in the number of proliferating crypts was observed in mice treated with 1,2-PD 1 h after irradiation. These findings suggested that 1,2-PD served as a radioprotector rather than a radiation mitigator. Subsequently, the effective dose of 1,2-PD for intestinal radioprotection was explored. It was found that the optimal dose for

intraperitoneal injection of 1,2-PD was 6 g/kg in mice (Supplementary Fig. 1C and 1D). Meanwhile, the time and dose effect of 1,2-PD per oral (p.o.) was examined. The results showed that 1,2-PD p.o. presented a similar time window as 1,2-PD i.p. injection. Besides, the best radioprotective effect was achieved 3 h before irradiation (Supplementary Fig. 1E and 1F). The optimal dose of 1,2-PD p.o. was 12 g/kg (Supplementary Fig. 1G and 1H). In general, the best enteric radioprotection performance could be achieved by i.p. injection of 6 g/kg 1,2-PD or application of 12 g/kg 1,2-PD p.o. to mice 3 h before irradiation. In all subsequent procedures, all mice received intraperitoneal administration of 6 g/kg of 1,2-PD 3h before irradiation unless otherwise specified.

To further evaluate the protective effect of 1,2-PD on radiation-induced intestinal injury, mice were intraperitoneally administered a single dose of 1,2-PD at 6g/kg 3 h before 15 Gy TBI. Histologic analysis of jejunum on day 3.5 after irradiation demonstrated a destruction of crypt-villus architecture with significant denudation of villus height (Fig. 1A, B). In contrast, 1,2-PD administration significantly increased intestinal villus ($P < 0.0001$) and crypt length ($P < 0.0001$) compared to the IR group (Fig. 1A-C). The BrdU IHC staining results showed that the number of proliferating crypts in the IR group decreased sharply from 135.06 ± 6.72 to 18.73 ± 3.49 at day 3.5 comparing to the blank group, while the number of proliferating crypts in the 1,2-PD treated group was approximately 3 times higher than that in the IR

group (Fig. 1D and 1E). We also employed the FITC-Dextran assay to evaluate the effect of 1,2-PD on the intestinal permeability of mice after irradiation. 1,2-PD administration significantly reduced FITC-Dextran levels in the serum of mice at day 3.5 after 12 Gy radiation ($P = 0.0138$) (Fig. 1F), indicating restitution of intestinal epithelial integrity by 1,2-PD treatment. The results above suggested that 1,2-PD potently ameliorated intestinal injury after TBI.

1,2-PD increases the survival of mice with RIGS following lethal irradiation doses.

To further confirm the protective effect of 1,2-PD on RIGS mice model, we first monitored the survival of mice after 12 Gy TBI. We found that the mice in the IR group began to die at day 4 and all mice died within 7 days after irradiation, which was match for typical lethal RIGS timeline (Fig. 2A). Meanwhile, 1,2-PD treated animal survived significantly longer, demonstrating an apparent radioprotective effect ($P < 0.0001$). As it has been reported that 1,2-PD has a radioprotective effect on the hematopoietic system [16]. To exclude the hematopoietic system protective effect, we conducted additional survival experiments using the total abdominal irradiation (TAI) model and 16 Gy TBI model combined with bone marrow transplantation (BMT). In TAI model of 15 Gy and 16 Gy, 1,2-PD significantly enhanced their survival, the survival rates after 30 days were 100% and 77.8%

respectively ($P = 0.0002$ and $P = 0.0033$, respectively) (Fig. 2B). The IR plus BMT group encounter rapidly full mortality within 7 days. In contrast, all 1,2-PD treated IR plus BMT group survived at least 30 days after treatment ($P < 0.0001$). We then gradually raised the radiation dose to 17-18 Gy, and it was discovered that 1,2-PD treated IR plus BMT group dose tolerance is to 18 Gy with a survival rate of 77.8%, while those not administrated with 1,2-PD suffered completely mortality in 7 days ($P = 0.0015$) (Fig. 2C). Besides, oral administration of 1,2-PD was also effective in increasing the survival rate of mice with 16 Gy TBI plus BMT ($P = 0.0063$) (Fig. 2D).

1,2-PD improves ISCs survival and facilitates crypt regeneration in mice and intestinal organoids.

Considering the dominant role of ISCs in the recovery of radiation injury, we examined the effects of 1,2-PD on ISCs after irradiation. Using IHC for Olfm4, we found that radiation caused a continuous loss of ISCs, with up to approximately 90% loss by 48 h post-irradiation, which were significantly suppressed in the 1,2-PD treated group. It was not until 3.5 days after irradiation that apparent proliferation and regeneration of surviving crypts were observed, which was particularly more evident in the 1,2-PD treated group than the IR group (Fig. 3A, B). To evaluate the radioprotective effect of 1,2-PD on the Lgr5⁺CBCs cells, we used Lgr5-EGFP-IRES-CreERT2 mice. The results showed that the expression of Lgr5-EGFP fluorescent protein was

rarely observed in the crypt of both groups 3.5 days after irradiation, but at day 5 post-irradiation, the number of Lgr5-EGFP⁺ ISCs in the crypt was increased in the 1,2-PD treated group comparing to the IR group (Fig. 3C, D). We also performed Lgr5 mRNA in situ hybridization (ISH) and Lysozyme IHC staining in mice intestine, and found a strong protection of Lgr5⁺ ISCs and Lysozyme⁺ Paneth cells in 1,2-PD treated group at day 3.5 after 14 Gy TBI (Fig. 3E, F, Supplementary Fig. 2). To further explore the effect of 1,2-PD on ISC proliferation and regeneration after irradiation, we performed in vitro intestinal organoids culture. And then the organoids were exposed to 0 or 4 Gy irradiation with or without 1,2-PD treatment. The results showed that the organoids in 1,2-PD treated group were larger in size and higher in budding rate than in the IR group at day 5 after 4 Gy irradiation (Fig. 3G-I). These data above demonstrated that 1,2-PD confirms protection against the loss of ISCs and improves crypt regeneration after irradiation in mice and in intestinal organoids.

1,2-PD induces reversible cell cycle arrest in enterocytes prior to irradiation

Small molecule fatty alcohols, such as 1,2-PD, have been showed to possess the capacity to inhibit cellular DNA synthesis when employed as cryoprotectants for freezing embryonic cells. Considering 1,2-PD is a known cryoprotectants[17], it is expected that 1,2-PD might induce cell cycle arrest,

a phenomenon that could potentially facilitate the repair of damaged DNA in small intestinal stem cells[18]. As illustrated in Figure 4A, 1,2-PD treatment led to a significant G0/G1 phase cell cycle arrest in IEC-6 cells. Upon withdrawal of 1,2-PD after a 24-hour exposure to IEC-6 cells, the percentage of cells in the G0/G1 phase gradually returned to control levels within the next 24 h (Fig. 4A, B). Furthermore, 1,2-PD treatment induced a dose-dependent suppression of Rb phosphorylation at S807/811 (Fig. 4C). These results suggest that 1,2-PD-induced cell cycle arrest is concentration-dependent and reversible. To assess the impact of 1,2-PD on the proliferation of intestinal crypts, we employed BrdU staining to define cells undergoing mitosis in irradiated C57BL/6 mice. As previously described, a significant radioprotective effect of 1,2-PD was observed in intestinal crypts at 48 and 96h post-irradiation (Fig. 4D, E). However, saline control group displayed a remarkable presence of dividing crypt cells (2082 ± 198 BrdU+ cells/circumference, 16.00 ± 1.52 BrdU+ cells/per crypt), whereas fewer BrdU+ cells were detected in mice treated with 1,2-PD (1694 ± 106 BrdU+ cells/circumference, 11.60 ± 1.68 BrdU+ cells/per crypt) prior to radiation (Fig. 4D-G). These results indicate that 1,2-PD induces intestinal crypt cells into a reversible dormant proliferative state, which may potentially be more advantageous for the survival of ISCs following radiation[19].

1,2-PD reduces DNA double-strand breaks in vitro and in vivo.

The DNA damage level correlates with the number of generating crypts after irradiation[20]. To investigate the damaged DNA repairing effect of 1,2-PD, immunofluorescence (IF) staining of γ H2AX in the IEC-6 cell was performed at first. After exposure to 2 Gy X-ray, the γ H2AX foci in IEC-6 peaked within the first hour, but then the number kept declining. Compared with that in the IR group, the number of γ H2AX foci formed in the 1,2-PD-treated group was apparently reduced, which demonstrated that 1,2-PD could promote the repair of DSBs (Fig. 5A, B). Secondly, the formation of γ H2AX in mice crypts after irradiation of 14 Gy TBI was observed. The results suggested that the γ H2AX foci formed in the 1,2-PD-treated group were significantly less than those in the IR group in vivo 6 h after irradiation. However, there was no statistical difference between the two groups in the number of γ H2AX foci formed 24 h after irradiation of 14 Gy TBI (Fig. 5C, D). Given that γ H2AX is a recognized marker of DSB[21], and recruits repair and checkpoint proteins following radiation exposure[22], its reduction is highly likely to indicate a decrease in the initial extent of DNA damage.

1,2-PD alleviates IR-induced intestinal apoptosis.

High doses of irradiation can lead to widespread apoptosis in the crypt, especially in ISCs, damaging the intestine regeneration function[23]. To explore the effects of 1,2-PD on apoptosis after irradiation, TUNEL staining and caspase-3 IHC were carried out on intestinal crypts of mice 6 h and 24 h after 14 Gy TBI. The results revealed that the number of TUNEL⁺ cells in the

crypts of the 1,2-PD-treated group (3.12 ± 0.25) was one-fold less than that in the IR group (6.68 ± 0.30) 6 h after irradiation. Besides, 1,2-PD also remarkably reduced the number of TUNEL⁺ cells in crypts 24 h after irradiation ($P=0.003$) (Fig. 6A, B). During the process of evaluating TUNEL⁺ cells in crypts at Positions 1-10 6 h after irradiation, it was found that cell apoptosis was more intensified in the transit amplifying (TA) zone at Positions 5-7 than that in CBCs at Positions 1-3 (Fig. 6C, D). Similarly, the number of caspase-3⁺ cells in intestinal crypts was also dramatically decreased in the 1,2-PD treated group 6 h and 24 h after irradiation (Fig. 6E, F). These findings indicated that 1,2-PD effectively mitigated apoptosis in crypts after irradiation. Position 1 was defined as the two apical cells in the crypt (11). The apoptotic index in the TA zone (70%) was about 20% larger than that of CBCs (50.56%), and the difference was statistically significant ($P=0.0053$) (Supplementary Fig. 3). The above results indicated that cells in the TA zone were vulnerable to apoptosis induced by TBI, whereas CBCs were relatively radioresistant. Furthermore, 1,2-PD could notably inhibit apoptosis at both positions. The number of TUNEL⁺ cells per crypt declined from 2.08 ± 0.21 in the IR group to 0.97 ± 0.11 in the 1,2-PD-treated group at Positions 1-3, and from 2.93 ± 0.18 in the IR group to 1.72 ± 0.20 in the 1,2-PD-treated group at Positions 5-7 (Fig. 6E, F).

1,2-PD inhibiting the intestinal p53-PUMA pathway.

To clarify the hypothesis whether 1,2-PD attenuated crypt apoptosis primarily through the P53-PUMA pathway, proteins and RNAs were extracted separately from the intestinal epithelium of mice 6 h and 24 h after irradiation. The expression levels of P53 pathway-related proteins and mRNAs were then examined. The results demonstrated that 1,2-PD treatment blocked the activation of P53 and its targets, such as PUMA, BAX and P21 (Fig. 6G). RT-PCR also confirmed that 1,2-PD restrained the mRNA expression of P53 and its targets at transcriptional level (Fig. 6H). However, currently there are no other studies have demonstrated that 1,2-PD directly regulates p53. Notably, hypoxic conditions are anticipated to regulate the p53 response[24]; the observed reduction in p53 activity may merely reflect hypoxic-induced cellular adaptation, which is possible on lipid compounds[25], necessitating further investigation into its underlying mechanisms.

To further investigate the role of P53 in 1,2-PD-mediated intestinal radioprotection, the survival rate and the number of crypts regenerated were compared between the *p53*-KO mice treated by vehicle and 1,2-PD after irradiation. In survival experiments of the models irradiated by 15 Gy TAI, *p53*-KO mice showed increased radiosensitivity. The *p53*-KO mice in the vehicle-treated group all died within 4 days after exposure, and their survival curve was significantly different from that of the vehicle-treated WT group ($P=0.0067$). It indicated that *p53* deficiency aggravated mice intestinal damage

after irradiation. In the meantime, the survival rate of the 1,2-PD-treated *p53*-KO group was much lower than that of the 1,2-PD-treated WT group ($P = 0.0086$), but significantly higher than that of the vehicle-treated *p53*-KO group ($P = 0.0316$) (Fig. 7A). This meant that P53 contributed to, at least in part, the intestinal radioprotection effect of 1,2-PD. The results of BrdU IHC staining testing on *p53*-KO mice 3.5 days after irradiation further confirmed that p53 played a role in intestinal radioprotection, and the results were consistent with those of the survival experiments. The generating crypts in vehicle-treated *p53*-KO mice were fewer than those in vehicle-treated WT mice, which implied that the deficiency of p53 enhanced intestinal radiosensitivity. Besides, the proliferating crypts in 1,2-PD-treated *p53*-KO mice were fairly fewer than those in 1,2-PD-treated WT mice, but more than those in vehicle-treated *p53*-KO mice, suggesting that p53 loss suppressed 1,2-PD-enhanced crypt regeneration. (Fig. 7B and 7C). In conclusion findings only provided ambiguous evidence of p53's role in 1,2-PD-mediated radioprotection of mouse intestines.

1,2-PD may regulate cell cycle and hypoxia response genes to enhance intestinal radiation resistance

Due the uncertain of exact mechanism, we decided to explore the possible transcription signaling of how 1,2-PD promote intestinal radiation resistance, we have collected mice intestinal tissue (Control V.S. 1,2-PD treated 3h) for

RNA sequencing. In which result could be demonstrated that 1,2-PD effect possibly involved in multiple biological processes, including cell cycle regulation and hypoxic response.

RNA sequencing results have detailed the expression patterns of multiple genes, including E2f3, Cyclin D2, Hif3a and PPAR α . In which E2f3 belongs to the E2F transcription factor family, participating in the regulation of cell cycle-related gene expression, particularly during the G1/S transition[26]. E2f3 showed down regulation, which would promote cell cycle arrest, confirmed with our previously results (Figure 8A).

Furthermore, RNA sequencing results revealed genes closely associated with the hypoxic response, such as Hif2, and Hif3. These members of the hypoxia-inducible factor (HIF) family play a central role in cellular responses to hypoxic environments, adapting to low-oxygen conditions by regulating a series of genes involved in cellular metabolism, angiogenesis, and survival. In this particularly, we have observed an interesting phenomenon that in known hypoxia gene, Hif-2 and Hif-3 gene exhibited a significant up regulation (Figure 8A&B) which have not been reported before.

We have also observed that 1,2-PD treatment have significantly upregulate the PPAR α , which is abnormal since 1,2-PD is alcohols compound and

ethanol intake inhibits the expression and activity of PPAR α (Figure 8A&B)[27, 28].

We further validated the reliability of certain gene expression alterations identified in the RNA sequencing through Reverse Transcription quantitative Polymerase Chain Reaction experiments. Results demonstrated that, compared to the control group, mRNA levels of Hif-3 were significantly upregulated in the 1,2-PD-treated group, suggesting that 1,2-PD treatment may enhance cellular response to hypoxia. Concurrently, the expression levels of E2F3 and CCND2 genes were markedly reduced in the treated group, potentially further influencing cell cycle regulation (Figure 8B). Cyclin D2, primarily expressed during the G1 phase, is involved in regulating the transition from G1 to S phase of the cell cycle[29]. This likely contributed to the significant G0/G1 phase cell cycle arrest observed in 1,2-PD-treated IEC-6 cells.

These findings suggest that 1,2-PD treatment may modulate biological processes such as cell cycle progression, lipid metabolism and hypoxia stress responses.

Discussion

Previous studies also reported that 1,2-PD could protect stem cells against IR within the hematopoietic system by tuning down the oxidative stress and

apoptotic activities[16]. This study systematically evaluated the protective effect of 1,2-PD on RIGS. It was discovered that 1,2-PD significantly prolongs animal survival, protects Lgr5⁺ ISCs, promotes crypt regeneration, and reduces radiation-induced DNA damage and apoptosis. Although the data exhibit high consistency at the phenomenological level, the precise mechanism of action requires further clarification. In particular, whether its regulation of the p53 pathway is direct and whether it acts in a p53-dependent manner warrant in-depth investigation.

Firstly, this study established the optimal timing and dosage for 1,2-PD administration, revealing that intraperitoneal injection (6 g/kg) or oral gavage (12 g/kg) administered 3 hours prior to irradiation yielded the most effective results. This indicates its utility as a radiation protective agent rather than a repair agent. This time window aligns with the drug's mechanism of action, which involves inducing cell cycle arrest and reducing radiosensitivity. Through BrdU labelling, Lgr5-EGFP tracing, and organoid models, we further confirmed that 1,2-PD effectively protects ISCs and enhances crypt regenerative capacity, with particularly pronounced effects observed at 3.5 days post-irradiation.

In specifically, we found regional-specific apoptotic effects of ISCs in crypt, and the Lgr5 positive cells residing in the crypt Position 1-3 seems to be

more radioresistant comparing with the TAs and LRCs in the other section of the crypt. The Lgr5+ ISCs were regarded as a group of proliferative active stem cells who exert massive activities in maintaining cryptic homeostasis[4, 5, 30, 31], and was reported to be indispensable in the radiation-induced regeneration of intestine[11]. Here, our results suggested Lgr5+ ISCs are sensitive to the protection from 1,2-PD under the attack of IR. In addition, we also found less apoptosis in the crypt Position 4-7 when giving 1,2-PD before IR. The dominating cells in these areas are Bmi1 positive LRCs and TAs who were reported to be quiescent usually and turned to active state after IR[7, 10, 32]. The activities from these stem cells could not only maintain the number of crypt and villi but also help maintain the number of Lgr5 positive cell cluster.

Secondly, mechanistic studies revealed that 1,2-PD induced reversible G0/G1 phase arrest in intestinal epithelial cells, accompanied by decreased Rb protein phosphorylation levels. This state of cell cycle “quiescence” is thought to facilitate the completion of DNA repair preparations prior to radiation exposure, thereby reducing radiation-induced lethal damage. Concurrently, γ H2AX foci assays revealed that 1,2-PD reduced the number of early post-radiation DNA double-strand breaks, suggesting it might have mitigate the initial radiation damage.

Regarding cellular death mechanisms, we observed that 1,2-PD significantly inhibited radiation-induced crypt cell apoptosis, particularly in the TA (transition amplification) region where cells exhibit heightened radiation sensitivity. Through TUNEL and Caspase-3 staining, we confirmed that 1,2-PD reduced the number of apoptotic cells while also downregulating the expression of p53 and its downstream target genes PUMA, BAX, and p21. Considering the observed reduction in γ H2AX, indicating diminished DNA damage, it may partly account for the induced decrease in p53 transcription.

But given that p53 serves as a key regulator of radiation injury, its absence itself exacerbates intestinal damage. [33, 34], therefore, its knockout blurs the protective effect of 1,2-PD. Our research failed to demonstrate that 1,2-PD enhances intestinal radiation resistance by directly regulating p53, though it may indirectly influence p53 activity.

Furthermore, transcriptomic analysis and results indicate that 1,2-PD treatment significantly downregulates cell cycle-related genes such as E2F3 and Cyclin D2, whilst simultaneously upregulating hypoxia-responsive gene Hif-3a. The downregulation of E2F3 and Cyclin D2 aligns with the G0/G1 phase arrest phenotype, whilst the upregulation of Hif-3a may participate in regulating cellular adaptation to hypoxia and metabolic stress. Although Hif-1a showed no significant changes, the upregulation of Hif-2a and Hif-3a

suggests it may play a unique role in 1,2-PD-mediated radiation adaptation, which merits further investigation.

Although this study provides relatively comprehensive pathological and cytological evidence supporting the potential of 1,2-PD as an intestinal radioprotective agent, and identifies that this protective effect is associated with cell cycle regulation, significant limitations remain. Due to the small-molecule nature of 1,2-PD, its specific molecular targets remain unclear, and whether it has directly regulation of the p53 pathway is direct requires further validation.

However, 1,2-PD upregulation of Hif family presents a highly intriguing avenue for investigation, suggesting 1,2-PD could be a potential Hif-3 α activator beyond oleoylethanolamide. In fact, oleoylethanolamide activates not only Hif-3 α but also PPAR α [35], which is similar to the transcriptomic results for 1,2-PD, suggesting that lipid related metabolism via PPAR α may associate with Hif-3a. A comparable association has already been demonstrated for Hif-1a/ PPAR α , exhibiting a protective effect in ischaemic bowel disease[25]; Hif-2, confirmed participated in protects against radiation-induced gastrointestinal toxicity[36].

Hypoxia exerts complex regulatory effects on p53 expression, typically suppressing both its expression and activity under severe hypoxic conditions, this could be another reason apart from previously described reduced DSB.

This primarily occurs through the activation of the hypoxia-inducible factor HIF-1 α , which promotes p53 degradation or inhibits its transcriptional activity[37]. Concurrently, hypoxia may enhance P53 ubiquitination and degradation by activating E3 ubiquitin ligases such as MDM2[38], or reduce P53 phosphorylation and activation by inhibiting the ATM/ATR signalling pathway. However, under specific conditions—such as hypoxia coupled with DNA damage or mild hypoxia—P53 may conversely be activated, participating in cell cycle arrest or apoptosis[39]. This could explain the observed downregulation of p53 following 1,2-PD treatment. However, given that 1,2-PD retains its protective effects in p53 knockout animals, the protective effect of 1,2-PD and p53 downregulation likely represent two independent downstream events.

In summary, 1,2-PD, as a small-molecule compound already approved by the FDA for injectable formulations, exhibits excellent biocompatibility and safety[15]. This study systematically elucidates for the first time its protective effects and mechanisms in RIGS, thereby expanding its potential applications and providing both theoretical foundations and experimental evidence for the clinical development of novel radiation protection drugs. Its mechanism of radioprotection is a substantial reduction of radiation-induced damage rather than radio-mitigative activity. Given its FDA-verified injectable safety and convenient oral bioavailability, a single prophylactic dose could be administered 3 h before abdominal or pelvic radiotherapy to

lower the incidence of radiation enteropathy and allow higher or full-dose treatment completion. Future work should evaluate its use in combination with current protective agents. Future research may further focus on identifying the molecular targets of 1,2-PD, deepening understanding of its mechanisms of action, and exploring combined application strategies with other radiation protection agents.

Materials and methods

Animals

Male C57BL/6J mice (6-8 weeks, 20-25 g) were purchased from Beijing HFK Bioscience Co.; Lgr5-EGFP-IRES-CreERT2 (stock no. 008875) and p53-knockout (p53-KO, stock no. 002101) mice were obtained from The Jackson Laboratory. Animals were housed in SPF barrier facilities (22 ± 2 °C, 50-60 % humidity, 12 h light/dark cycle) with ad libitum access to standard chow and water. A 7-day acclimatization period was allowed before experimentation. The study protocol was approved by the Institutional Animal Care and Use Committee of the Beijing Institute of Radiation Medicine and was in line with ARRIVE guidelines 2.0.

Experimental Groups

Mice were randomly assigned to the following groups:

FIGURE NUMBER	EXPERIMENT	GROUP DESIGN	MICE PER GROUP	GROUPS	MICE
FIG.1A&D	Histology / BrdU (3.5d)	Sham; 15Gy TBI; 15Gy TBI+1,2-PD	3	3	9
FIG.1F	FITC-Dextran permeability	12Gy TBI; 12Gy TBI+1,2-PD	5	2	10
FIG.2A	Survival (12 Gy TBI)	12Gy TBI; 12Gy TBI+1,2-PD	10	2	20
FIG.2B	Survival (15-17 Gy TAI)	15, 16, 17Gy TAI; 15, 16, 17Gy TAI+1,2-PD	9	6	54
FIG.2C	Survival (16-18 Gy TBI + BMT)	16, 17, 18Gy TBI+BMT; 15, 16, 17Gy TBI+BMT+1,2-PD	9	6	54
FIG.2D	Oral survival (16 Gy TBI + BMT)	16Gy TBI+BMT; 16Gy TBI+BMT+1,2-PD(p.o.)	9	2	18
FIG.3A	Olfm4 IHC staining	14Gy TBI; 14Gy TBI+1,2-PD (0, 6, 24, 48h&3.5d)	3	10	30
FIG.3C	Lgr5-EGFP+ ISCs	12Gy TBI; 12Gy TBI+1,2-PD (0h &3, 3.5d)	3	6	12
FIG.3E	Lgr5 mRNA ISH	14Gy TBI; 14Gy TBI+1,2-PD (0h&3.5d)	3	4	12
FIG.4D,F	BrdU (different cycle time)	14Gy TBI; 14Gy TBI+1,2-PD (0, 8, 24, 48, 96h)	3	10	12
FIG.5C	γ H2AX assay (mice)	14Gy TBI; 14Gy TBI+1,2-PD (6, 24h)	3	4	12
FIG.6B	TUNEL	14Gy TBI; 14Gy TBI+1,2-PD (6, 24h)	3	4	12
FIG.6E,G	Caspase-3 IHC, WB	14Gy TBI; 14Gy TBI+1,2-PD (6, 24h)	3	4	12
FIG.7A	p53-KO survival	WT 14Gy TBI; WT 14Gy TBI+1,2-PD; P53KO 14Gy TBI; P53KO 14Gy TBI+1,2-PD	12	4	48

FIG.7B	p53-KO BrdU	WT 14Gy TBI; WT 14Gy TBI+1,2-PD; P53KO 14Gy TBI; P53KO 14Gy TBI+1,2-PD	3	4	12
FIG.8A&B	RNA-sequencing; RT-PCR	Control; 1,2-PD (3h)	3	2	6
TOTAL					333

Animal anesthesia and euthanasia: Animals are anesthetized with sodium pentobarbital at 70 mg kg⁻¹ via intraperitoneal injection before radiation exposure to allow proper positioning. Animals are euthanized by cervical dislocation performed by trained personnel before collect tissue samples.

Irradiation Procedure: TBI was delivered by a ⁶⁰Co source (Beijing Institute of Radiation Medicine) at 0.68 Gy min⁻¹ (12-18 Gy). TAI was performed with an X-ray biological irradiator Rad Source RS-2000 (220 kV, 25 mA, 15-17 Gy, 2.5 cm tissue-depth dose calibration, at maximum dose rate of 1.0 Gy/min). Animals were anaesthetized as above.

Drug Preparation and Administration: 1,2-PD (Sigma-Aldrich, ≥99 %) was diluted in sterile saline to 60 % (v/v) and administered i.p. at 6 g kg⁻¹ 3 h before irradiation. For oral dosing, 1,2-PD was prepared as 50 % (v/v) and given by gavage at 12 g kg⁻¹. Vehicle groups received equivalent volumes of saline.

Tissue Collection and Processing: Animals were euthanized at 6 h, 24 h, 3.5 days or 5 days post-irradiation. Jejunum (5 cm distal to the ligament of Treitz) was harvested.

H&E and BrdU staining. BrdU (Selleckchem, S7918) was intraperitoneally

injected 1 h before mice sacrifice at a dose of 120 mg/kg. Jejunum tissues were harvested at indicated time points, fixed in 4% PFA for 12 h and then embedded in paraffin, sections of 4 μ m thick were dewaxed and subjected to hematoxylin and eosin (H&E) staining for histological analysis. As for BrdU staining, tissue sections were treated with 2 M HCl and pepsin to fully expose BrdU antigenic epitopes.

FITC-dextran permeability assay: C57BL/6 mice were administered 6 mg/kg 1,2-PD or PBS on day 0 and day 3 after 12 Gy TBI. At day 3.5 post-irradiation, animals were gavaged with 150 μ L 80 mg/mL 4KDa FITC-Dextran(Sigma-Aldrich, St. Louis, MO) in sterile water, 3 hours after gavage, mice were killed and serum was obtained by cardiac puncture. Samples were transferred to black 96-well microplates. FITC-Dextran concentrations were analyzed with a fluorescence spectrophotometer and fluorescence intensity was measured (excitation, 492 nm; emission, 525 nm). A standard curve was constructed using mouse serum having increasing amounts of FITC-dextran to determine the serum levels of FITC-dextran in different treatment groups.

Immunohistochemistry (IHC) and immunofluorescence (IF). Paraffin-embedded sections (4 μ m) were dewaxed and rehydrated. Antigen retrieval was performed by boiling the sections in pH6.0 10 mM citrate buffer with a microwave oven for 15 min. For IHC, sections were treated to block endogenous peroxidase. As for IEC-6 immunofluorescence, cells were cultured on coverslips placed in 6-well plates and adhered overnight.

Subsequently, the cells were fixed with 4% PFA and permeabilized with 0.5% Triton X-100/PBS for 30 min each. And all sections of IHC and IF were incubated with sequestering serum or 5% BSA to block non-specific-binding sites. Primary antibody was incubated overnight at 4°C, followed by incubation of the secondary antibody for 1 h at 37°C. The antibodies used were as follows: Olfm4 (CST,39141), EGFP (CST,2956S), γ H2AX (Millipore, Cat.05-636-1), Caspase-3 (CST,9661), BrdU (ZSGB-BIO, ZM-0013), DyLight 488 (Abbkine, A23210).

TUNEL assay. The 3 μ m-thick of paraffin-embedded sections were performed according to the manufacturer's protocols (Beyotime, C1098). The apoptotic cell numbers per crypt were quantified by counting TUNEL⁺ cells in 30 consecutive intact crypts of each mouse, and the apoptotic index of each position in crypt was calculated as the percentage of the frequency of TUNEL⁺ cells in 20 consecutive intact crypts per mice. Three mice were used in each group.

Single-cell-resolution imaging of EGFP in Lgr5-EGFP-IRES-CreERT2 mice. Tracing the fate of Lgr5-EGFP⁺ cells in their three-dimensional near-native environment was performed as previously described. Briefly, intestinal tissues of Lgr5-EGFP-IRES-CreERT2 mice were embedded in 4% low melting point agarose(LMA) gel and sectioned with a vibrating blade microtome(Campden Instruments, 5100mz). The settings of vibrating blade microtome were as follows: slicing thickness:150 μ m, velocity:2 mm/s, knife amplitude:0.9 mm

and vibration frequency:65 Hz. The near-native sections were penetrated in PBD0.2T for 90 min at room temperature and stained with DAPI. Then, sections were immediately observed under a laser confocal microscope (Nikon A1, Japan).

In situ hybridization (ISH). RNAscope® 2.5HD Detection Reagent-RED (322360) and Lgr5 probe (312171) were purchased from Advanced Cell Diagnostics (ACD). ISH for Lgr5 was performed according to the manufacturer's instructions. For the quantification analysis of ISH results, number of stained spots in 5 consecutive complete crypts were counted in every mouse, and there were 3 mice in each group.

Analysis of cell cycle distribution. Cells were washed twice with PBS and subsequently fixed with ice-cold 70% ethanol, allowing fixation to occur overnight at 4°C. Following fixation, the cells were rinsed with PBS, treated with 1% RNase A for a minimum of 15 minutes at 37°C, and subsequently stained with 50 µg/ml of propidium iodide (PI). The stained cells were then subjected to flow cytometry analysis. The acquired data were subsequently analyzed using CELLQuest software.

Culture and treatment of intestinal organoids in vitro. The small intestinal crypts of mice were isolated and cultured in vitro as previously described[40, 41]. In brief, the small intestine was dissected longitudinally, washed in PBS until clear and cut into 2-5 mm segments, rocked with 2 mM EDTA on ice for 30 min and followed by vigorous vertical shaking

approximately 50 times, left it on ice for 2-3 min before discarding the supernatant. Then it was gently blown with 10% FBS-PBS 3-5 times and the upper suspension was collected by passing through a 75- μ m filter. The suspension was then centrifuged at 290 g for 5 min at 4°C. About 200 crypts were resuspended in 50 μ l organoids growth medium (StemCell,06005) and Matrigel (Corning,356231) mixture, and then planted in a prewarmed 24-well plate. The plate was put in the 37°C incubator for 30 minutes and added 500 μ l organoids growth medium. The culture medium was refreshed every 3 days. Prior to radiation exposure, 1,2-PD was incubated for 6 hours at a concentration of 2% v/v. Immediately following irradiation, the medium was replaced with normal medium to eliminate the presence of 1,2-PD.

Analysis of protein and mRNA expression. Protein and mRNA lysates from mice intestinal epithelial cells were obtained by TRIzol reagent method, and protein extraction of IEC-6 was performed as previously described[42]. Protein extracts were subjected to SDS-PAGE gel electrophoresis and Western blotting analysis. The antibodies used were as follows: P53 (CST, 2524S), PUMA (Proteintech, 55120-1-AP), BAX (CST, 2772T), P21 (CST, 2947T), GAPDH (Proteintech, 60004-1-Ig). RT-PCR was performed to detect corresponding target gene transcript levels; primers were listed here:

Gene	Primer	Sequence
P53	Forward Primer	TGAAACGCCGACCTATCCTTA
	Reverse Primer	GGCACAAACACGAACCTCAAA
PUMA	Forward Primer	ATGGCGGACGACCTCAAC

	Reverse Primer	AGTCCCATGAAGAGATTGTACATGAC
Bax	Forward Primer	GGGTTGTCGCCCTTTTCTACTT
	Reverse Primer	AGCCCATGATGGTTCTGATCA
P21	Forward Primer	ATGTCCAATCCTGGTGATGT
	Reverse Primer	TGCAGCAGGGCAGAGGAAGT
GAPDH	Forward Primer	CTCTGGAAAGCTGTGGCGTGATG
	Reverse Primer	ATGCCAGTGAGCTTCCCGTTCAG
HIF1	Forward Primer	ACCTTCATCGGAAACTCCAAAG
	Reverse Primer	ACTGTTAGGCTCAGGTGAACT
HIF2	Forward Primer	CTGAGGAAGGAGAAATCCCGT
	Reverse Primer	TGTGTCCGAAGGAAGCTGATG
HIF3	Forward Primer	GAAGTTCACATACTGCGACGA
	Reverse Primer	GTCCAAAGCCTGGATGTATTCAT
CCND2	Forward Primer	CCTGGATGCTAGAGGTCTGTG
	Reverse Primer	GGCCTTAGTGTGATGGGGAA
E2F3	Forward Primer	AAACGCGGTATGATACGTCCC
	Reverse Primer	CCATCAGGAGACTGGCTCAG
PPAR α	Forward Primer	CTGCTCGAAGCACCCCTTACC
	Reverse Primer	TCCTGAGGATGGGACATTTTCA

Bone marrow transplantation:

(1) Recipient mice were euthanised after total-body irradiation (TBI) with a lethal dose of γ -rays, and the whole body was disinfected with 75 % (v/v) ethanol. (2) Under aseptic conditions in a Class II biological safety cabinet, both femora were dissected and the epiphyses were pierced with a sterile 1-mL syringe needle. (3) The marrow cavity was flushed with ice-cold RPMI-

1640 medium (Gibco, USA) until the bones appeared blanched; the flushate was gently aspirated through the same needle to minimise cell clumping. (4) The pooled flushate was centrifuged at $500 \times g$ for 5 min at 4 °C, the supernatant was discarded, and the cell pellet was resuspended in fresh RPMI-1640 to obtain a single-cell bone-marrow suspension. (5) A 20- μ L aliquot was loaded into a haemocytometer for total nucleated cell counting; the suspension was then adjusted to 2.5×10^7 cells mL^{-1} in RPMI-1640. (6) Six hours post-TBI, recipient mice received 5×10^6 bone-marrow cells in 200 μ L RPMI-1640 via lateral tail-vein injection.

Inclusion / exclusion criteria:

Mice were included only if they met the following pre-established criteria: (i) body weight within 20-25 g, (ii) normal baseline stool consistency, and (iii) completion of the full radiation protocol. Animals showing wound infection, anaesthesia-related mortality within 24 h, or technical failure of irradiation were pre-specified for exclusion. No animals or data points were excluded from the final analyses.

Randomization and blinding:

Group allocation was randomized by a computer-generated random sequence stratified by body weight. Cage position on the rack and order of procedures were rotated daily to minimize environmental confounders. Cage location and order of procedures were randomized across groups to eliminate spatial and temporal biases. Investigators performing histological scoring, organoid

imaging, and survival checks were blinded to treatment allocation; blinding was broken only after final data lock.

RNA sequencing:

Total RNA was extracted from freshly isolated intestinal crypts of C57BL/6 mice at 3 hours post 1,2-PD treatment using TRIzol reagent (Invitrogen, USA) according to the manufacturer's instructions. RNA integrity was assessed using an Agilent 2100 Bioanalyzer (Agilent Technologies, USA), and samples with RNA Integrity Number (RIN) ≥ 7.0 were selected for subsequent analysis.

After RNA quality control, mRNA was enriched from total RNA using HiFFNGS™ mRNA Isolation Master Kit (Yeasen, Cat#12603) with oligo(dT)-conjugated magnetic beads. The enriched mRNA was then fragmented into short pieces using fragmentation buffer. First-strand cDNA was synthesized using random hexamer primers, followed by second-strand synthesis with dNTPs, RNase H, and DNA Polymerase I. The resulting double-stranded cDNA was subjected to end repair, A-tailing, and ligation of sequencing adapters. After adapter ligation, the cDNA libraries were amplified by PCR and purified. The final libraries were quantified using a Qubit Fluorometer (Thermo Fisher Scientific) and assessed for fragment size distribution using an Agilent 2100 Bioanalyzer (Agilent Technologies). Libraries that passed quality control were used for sequencing. Paired-end sequencing (150 bp)

was performed on the DNBSEQ-T7 platform (BGI, China). On average, approximately 10.27 Gb of clean data were generated per sample.

Statistics. Statistical analysis was performed using GraphPad Prism 8.0 software. Data are presented as means \pm SD or means \pm SEM. For multiple group comparisons (e.g., Figures 6D and 7C), one-way ANOVA was applied followed by Tukey's honestly significant difference (HSD) post hoc test for pairwise comparisons. Dunnett's test was used when all groups were compared against a single control group. Survival curves were analyzed using the log-rank test. A P value of less than 0.05 was considered statistically significant.

References

1. Hauer-Jensen M, Denham JW, Andreyev HJ: **Radiation enteropathy--pathogenesis, treatment and prevention.** *Nat Rev Gastroenterol Hepatol* 2014, **11**:470-479.
2. Kirsch DG, Santiago PM, di Tomaso E, Sullivan JM, Hou WS, Dayton T, Jeffords LB, Sodha P, Mercer KL, Cohen R, et al: **p53 controls radiation-induced gastrointestinal syndrome in mice independent of apoptosis.** *Science* 2010, **327**:593-596.
3. Takeda N, Jain R, LeBoeuf MR, Wang Q, Lu MM, Epstein JA: **Interconversion between intestinal stem cell populations in distinct niches.** *Science* 2011, **334**:1420-1424.
4. Li L, Clevers H: **Coexistence of quiescent and active adult stem cells in mammals.** *Science* 2010, **327**:542-545.
5. Barker N, van Es JH, Kuipers J, Kujala P, van den Born M, Cozijnsen M, Haegbarth A, Korving J, Begthel H, Peters PJ, Clevers H: **Identification of stem cells in small intestine and colon by marker gene Lgr5.** *Nature* 2007, **449**:1003-1007.
6. Schuijers J, van der Flier LG, van Es J, Clevers H: **Robust cre-mediated recombination in small intestinal stem cells utilizing the olfm4 locus.** *Stem Cell Reports* 2014, **3**:234-241.
7. Sangiorgi E, Capecchi MR: **Bmi1 is expressed in vivo in intestinal stem cells.** *Nat Genet* 2008, **40**:915-920.
8. Munoz J, Stange DE, Schepers AG, van de Wetering M, Koo BK, Itzkovitz S,

- Volckmann R, Kung KS, Koster J, Radulescu S, et al: **The Lgr5 intestinal stem cell signature: robust expression of proposed quiescent '+4' cell markers.** *EMBO J* 2012, **31**:3079-3091.
9. Barker N, van Oudenaarden A, Clevers H: **Identifying the stem cell of the intestinal crypt: strategies and pitfalls.** *Cell Stem Cell* 2012, **11**:452-460.
 10. Tian H, Biehs B, Warming S, Leong KG, Rangell L, Klein OD, de Sauvage FJ: **A reserve stem cell population in small intestine renders Lgr5-positive cells dispensable.** *Nature* 2011, **478**:255-259.
 11. Metcalfe C, Kljavin NM, Ybarra R, de Sauvage FJ: **Lgr5+ stem cells are indispensable for radiation-induced intestinal regeneration.** *Cell Stem Cell* 2014, **14**:149-159.
 12. Leibowitz BJ, Qiu W, Liu H, Cheng T, Zhang L, Yu J: **Uncoupling p53 functions in radiation-induced intestinal damage via PUMA and p21.** *Mol Cancer Res* 2011, **9**:616-625.
 13. Sullivan JM, Jeffords LB, Lee CL, Rodrigues R, Ma Y, Kirsch DG: **p21 protects "Super p53" mice from the radiation-induced gastrointestinal syndrome.** *Radiat Res* 2012, **177**:307-310.
 14. Qiu W, Carson-Walter EB, Liu H, Epperly M, Greenberger JS, Zambetti GP, Zhang L, Yu J: **PUMA regulates intestinal progenitor cell radiosensitivity and gastrointestinal syndrome.** *Cell Stem Cell* 2008, **2**:576-583.
 15. Ruddick JA: **Toxicology, metabolism, and biochemistry of 1,2-propanediol.** *Toxicol Appl Pharmacol* 1972, **21**:102-111.
 16. Yi L, Tian M, Piao C, Gao G, Wu L, Pan Y, Liu J: **The protective effects of 1,2-propanediol against radiation-induced hematopoietic injury in mice.** *Biomed Pharmacother* 2019, **114**:108806.
 17. Whaley D, Damyar K, Witek RP, Mendoza A, Alexander M, Lakey JR: **Cryopreservation: An Overview of Principles and Cell-Specific Considerations.** *Cell Transplant* 2021, **30**:963689721999617.
 18. Weeden CE, Asselin-Labat ML: **Mechanisms of DNA damage repair in adult stem cells and implications for cancer formation.** *Biochim Biophys Acta Mol Basis Dis* 2018, **1864**:89-101.
 19. Wei L, Leibowitz BJ, Wang X, Epperly M, Greenberger J, Zhang L, Yu J: **Inhibition of CDK4/6 protects against radiation-induced intestinal injury in mice.** *J Clin Invest* 2016, **126**:4076-4087.
 20. Yuan Q, Peng R, Yu H, Wang S, Chen Z, Dong S, Li W, Cheng B, Jiang Q, Cong Y, et al: **Disulfiram Protects Against Radiation-Induced Intestinal Injury in Mice.** *Front Pharmacol* 2022, **13**:852669.
 21. Rogakou EP, Pilch DR, Orr AH, Ivanova VS, Bonner WM: **DNA double-stranded breaks induce histone H2AX phosphorylation on serine 139.** *J Biol Chem* 1998, **273**:5858-5868.
 22. Prabhu KS, Kuttikrishnan S, Ahmad N, Habeeba U, Mariyam Z, Suleman M, Bhat AA, Uddin S: **H2AX: A key player in DNA damage response and**

- a promising target for cancer therapy. *Biomed Pharmacother* 2024, **175**:116663.
23. Chang PY, Qu YQ, Wang J, Dong LH: **The potential of mesenchymal stem cells in the management of radiation enteropathy.** *Cell Death Dis* 2015, **6**:e1840.
24. Achison M, Hupp TR: **Hypoxia attenuates the p53 response to cellular damage.** *Oncogene* 2003, **22**:3431-3440.
25. Li L, Liu Y, Zhi N, Ji Y, Xu J, Mao G, Wang Y, Ma J, Wang Y: **Hypoxic preconditioning accelerates the healing of ischemic intestinal injury by activating HIF-1 α /PPAR α pathway-mediated fatty acid oxidation.** *Cell Death Discovery* 2024, **10**:164.
26. Leone G, DeGregori J, Yan Z, Jakoi L, Ishida S, Williams RS, Nevins JR: **E2F3 activity is regulated during the cell cycle and is required for the induction of S phase.** *Genes Dev* 1998, **12**:2120-2130.
27. Nan YM, Wang RQ, Fu N: **Peroxisome proliferator-activated receptor α , a potential therapeutic target for alcoholic liver disease.** *World J Gastroenterol* 2014, **20**:8055-8060.
28. Yue R, Chen GY, Xie G, Hao L, Guo W, Sun X, Jia W, Zhang Q, Zhou Z, Zhong W: **Activation of PPAR α -catalase pathway reverses alcoholic liver injury via upregulating NAD synthesis and accelerating alcohol clearance.** *Free Radic Biol Med* 2021, **174**:249-263.
29. Sherr CJ: **D-type cyclins.** *Trends Biochem Sci* 1995, **20**:187-190.
30. Yan KS, Chia LA, Li X, Ootani A, Su J, Lee JY, Su N, Luo Y, Heilshorn SC, Amieva MR, et al: **The intestinal stem cell markers Bmi1 and Lgr5 identify two functionally distinct populations.** *Proc Natl Acad Sci U S A* 2012, **109**:466-471.
31. Koo BK, Clevers H: **Stem cells marked by the R-spondin receptor LGR5.** *Gastroenterology* 2014, **147**:289-302.
32. Zhu Y, Huang YF, Kek C, Bulavin DV: **Apoptosis differently affects lineage tracing of Lgr5 and Bmi1 intestinal stem cell populations.** *Cell Stem Cell* 2013, **12**:298-303.
33. Merritt AJ, Potten CS, Kemp CJ, Hickman JA, Balmain A, Lane DP, Hall PA: **The role of p53 in spontaneous and radiation-induced apoptosis in the gastrointestinal tract of normal and p53-deficient mice.** *Cancer Res* 1994, **54**:614-617.
34. Wang J, Chang C-Y, Yang X, Zhou F, Liu J, Bargonetti J, Zhang L, Xie P, Feng Z, Hu W: **p53 suppresses MHC class II presentation by intestinal epithelium to protect against radiation-induced gastrointestinal syndrome.** *Nature Communications* 2024, **15**.
35. Diao X, Ye F, Zhang M, Ren X, Tian X, Lu J, Sun X, Hou Z, Chen X, Li F, et al: **Identification of oleoylethanolamide as an endogenous ligand for HIF-3 α .** *Nature Communications* 2022, **13**.
36. Taniguchi CM, Miao YR, Diep AN, Wu C, Rankin EB, Atwood TF, Xing L, Giaccia AJ: **PHD inhibition mitigates and protects against radiation-**

- induced gastrointestinal toxicity via HIF2.** *Sci Transl Med* 2014, **6**:236ra264.
37. Ravi R, Mookerjee B, Bhujwalla ZM, Sutter CH, Artemov D, Zeng Q, Dillehay LE, Madan A, Semenza GL, Bedi A: **Regulation of tumor angiogenesis by p53-induced degradation of hypoxia-inducible factor 1alpha.** *Genes Dev* 2000, **14**:34-44.
 38. Chen D, Li M, Luo J, Gu W: **Direct Interactions between HIF-1 α and Mdm2 Modulate p53 Function*.** *Journal of Biological Chemistry* 2003, **278**:13595-13598.
 39. Zhao Y, Chen XQ, Du JZ: **Cellular adaptation to hypoxia and p53 transcription regulation.** *J Zhejiang Univ Sci B* 2009, **10**:404-410.
 40. Mahe MM, Aihara E, Schumacher MA, Zavros Y, Montrose MH, Helmrath MA, Sato T, Shroyer NF: **Establishment of Gastrointestinal Epithelial Organoids.** *Curr Protoc Mouse Biol* 2013, **3**:217-240.
 41. Qu M, Xiong L, Lyu Y, Zhang X, Shen J, Guan J, Chai P, Lin Z, Nie B, Li C, et al: **Establishment of intestinal organoid cultures modeling injury-associated epithelial regeneration.** *Cell Res* 2021, **31**:259-271.
 42. Li M, Lang Y, Gu MM, Shi J, Chen BPC, Yu L, Zhou PK, Shang ZF: **Vanillin derivative VND3207 activates DNA-PKcs conferring protection against radiation-induced intestinal epithelial cells injury in vitro and in vivo.** *Toxicol Appl Pharmacol* 2020, **387**:114855.

Acknowledgements

We thank Professor Yuwen Cong for his generous gift of Lgr5-EGFP-IRES-CreERT2 mice. We also thank Goulin Xiong and Yin Xu for their technical assistance in experiments. The authors declare no use of Artificial Intelligence in this study.

Conflict of Interest Statement

There are no ethical/legal conflicts involved in the article.

Animal Ethics declaration

The research was carried out in accordance with the approval of the ethics

committee. Studies involving animal experiment were approved by the Institutional Animal Care and Use Committee of the Beijing Institute of Radiation Medicine. The approval project title is "Mechanism Study of Propylene Glycol in the Prevention and Treatment of Intestinal Acute Radiation Syndrome". The permit number is "Ethics Review Approval no. IACUC-DWZX-2020-599", which issued at April 15, 2025. All protocols followed are compliant with specific ethical regulations.

Author Contribution Statement

Ying Jiang and Xing Shen designed this study and conducted the main analysis. Jiwei Zhao, Chunan Zhao, Ying Jiang, Xing Shen, Aoqiang Ji and Xun Wang performed the experiments. Chunan Zhao wrote and edited the manuscript. Zuyin Yu, Gang Sun, Shuang Xing and Yuwen Cong provided additional expertise. Xing Shen, He Xiao, Zuyin Yu reviewed and edited the article. All authors contributed to the article and approved the submitted version.

Funding Statement

This research received no specific grant from funding agencies in the public, commercial, or not-for-profit sectors.

Data Availability Statement

The datasets used and/or analyzed during the current study are available from the corresponding author on reasonable request. The raw RNA-seq data reported in this study have been deposited in the NCBI Sequence Read Archive (SRA) under BioProject accession number PRJNA1358381.

Figure legends

Figure 1. 1,2-PD promotes crypt proliferation and intestine structural preservation 3.5 days after 15 Gy TBI. (A) Representative images of H&E-stained intestinal sections from each group at day 3.5. (B) Villus height in each group at day 3.5. (C) Crypt depth in each group at day 3.5. (D) Representative images of each group for proliferative crypts in mice 3.5 days after 15 Gy TBI. (E) Quantification of proliferative crypts per circumference. A crypt containing more than 5 BrdU⁺ cells is recognized as a proliferating crypt. (F) The FITC-Dextran levels in the serum of mice at day 3.5 after 12 Gy TBI. Values represent the *mean* ± *SD*. *N* = 5 mice in each group. (A and C) Scale bars: 500 μm (top) and 200 μm(bottom). (B, C and D) Values represent the *mean* ± *SD*. *N* = 3 mice in each group. ****P* < 0.001. **P* < 0.05.

Figure 2. 1,2-PD protects mice from lethal doses of irradiation. (A) Kaplan-Meier survival curves of mice (n = 10/group) after 12 Gy TBI. (B) Kaplan-Meier survival analysis of mice (n = 9/group) after 15-17 Gy TAI in each

group. (C) Kaplan-Meier survival curves of mice ($n = 9/\text{group}$) subjected to lethal doses (16-18 Gy) of TBI combined with BMT in each group, with or without 1,2-PD treatment. (D) Mice were treated with 1,2-PD (p.o.) (12 mg/kg body weight) at 3 h before irradiation. Kaplan-Meier survival curves of mice ($n = 9/\text{group}$) subjected to 16Gy of TBI combined with BMT in each group group. Values are represented by the *mean* \pm *SD*. *** $P < 0.001$.

Figure 3. 1,2-PD confirms protection against the loss of ISCs and improves crypt regeneration post-irradiation. (A) Representative images of Olfm4 IHC in the crypts after 14 Gy TBI. (B) Quantification of Olfm4⁺ ISCs per crypt at the indicated time points. (C) Representative confocal images of Lgr5-EGFP⁺ ISCs in the crypts after 12 Gy TBI. (D) Quantification of Lgr5-EGFP⁺ ISCs per field at the indicated time points. (E) Representative images of Lgr5 mRNA ISH in the crypts after 14 Gy TBI. (F) Quantification of Lgr5⁺ mRNA staining per crypt. (G) Representative morphology of intestinal organoids at day 5 after 0 or 4 Gy irradiation with or without 1,2-PD pretreatment. (H) Quantification of budding rates in each group. (I) Quantification of budding numbers per organoid in each group. (A, C and E) Scale bar:100 μm , (G) Scale bar:200 μm . (B, D, F, H and I) Values represent the *mean* \pm *SEM*. (B, D and F) $N = 3$ mice in each group. (H and I) $N = 60$ intestinal organoids from each group. * $P < 0.05$, ** $P < 0.01$, *** $P < 0.001$.

Figure 4. 1,2-PD induces cell cycle arrest in enterocytes in vivo and in vitro. (A, B) IEC-6 cells were incubated with 2% 1,2-PD for 24 h, and the medium was replaced with fresh medium for an additional 24 hours. Cells were harvested at 12 and 24 h after 1,2-PD treatment, as well as 12 and 24 h after 1,2-PD withdrawal. Subsequently, DNA content in the cells was assessed through flow cytometry analysis. (A) Representative histograms of propidium-labeled cells analyzed by flow cytometry. (B) Percentage of cells in the G0/G1 phase of the cell cycle. The values are presented as the mean \pm SD of three independent experiments. $*P < 0.05$, $**P < 0.01$. (C) IEC-6 cells were stimulated with 0% \square 0.5% \square 1% or 2% 1,2-PD for 24 h. The cell lysates were used in immunoprecipitations with antibodies to Rb phosphorylated on S807/S811, S780 or S795. (D-G) Mice were pre-treated with either vehicle or 1,2-PD and then exposed to 14 Gy total body irradiation (TBI). The small intestine was analyzed at specified time points. (D) Representative images of BrdU-stained sections of the intestinal tissue. Scale bar: 200 μm . (E) Quantification of BrdU+ crypt cells per circumference in (D). (F) Representative images of BrdU immunohistochemistry (IHC) in crypts at 0, 8, and 24 h. Scale bar: 20 μm . (G) Quantitation of BrdU+ crypt cells in (F). Values represent the mean \pm SD. (F and G) $N = 3$ mice in each group. $*P < 0.05$, $***P < 0.001$.

Figure 5 1,2-PD reduces DNA DSBs in vitro and in vivo. (A) Representative

confocal IF images of γ H2AX foci in IEC-6 treated with 1,2-PD or vehicle after irradiation of 2 Gy X-ray. (B) Quantification of γ H2AX foci per nucleus at the indicated time points after irradiation. (C) Representative confocal IF images of γ H2AX foci in crypts treated with 1,2-PD or vehicle after 14 Gy TBI. (D) Quantification of the area ratio of γ -H2AX foci per field at the indicated time points. (A) Scale bar: 25 μ m. (C) Scale bar: 50 μ m. (B) Values are represented by the *mean* \pm *SEM* from 3 independent experiments. (D) Values are represented by the *mean* \pm *SEM*, *N*=3 mice in each group. **P*<0.05, ***P*<0.01, ****P*<0.001.

Figure 6. 1,2-PD alleviates IR-induced intestinal apoptosis by inhibiting the p53-PUMA signal pathway. (A) Representative images of TUNEL staining in intestinal sections at indicated time points after 14 Gy TBI. (B) Quantification of TUNEL⁺ cells in crypts at indicated time points after 14 Gy TBI. (C) and (D) Quantification of TUNEL⁺ cells in crypts and per crypt at Positions 1-10 6h after 14 Gy TBI, respectively. (E) Representative images of caspase-3 IHC in intestinal sections at indicated time points after 14 Gy TBI. (F) Quantification of caspase-3⁺ cells in crypts at indicated time points after 14 Gy TBI. (G) Western blotting analysis of the intestinal expression of the P53 pathway-related proteins. GAPDH was used as the loading control. (H) Intestinal expression of the P53 pathway-related mRNAs in the experimental and control mice 6 h after irradiation. (A and E) Scale bar: 50 μ m. (B, C, D and F)

30 crypts were counted in each mouse, N =3 mice in each group. (G and H) Results were obtained from 3 independent experiments. Values are represented by the *mean* \pm *SEM*. **P* <0.05, ***P* <0.01, ****P* <0.001.

Figure 7. P53 acts as a radioresistant factor and 1,2-PD mediates radioprotection of mouse intestines partly via the P53 signaling pathway. (A) Kaplan-Meier survival curve of P53 gene-edited mice treated with vehicle or 1,2-PD after 14Gy TBI. (B) Representative images of BrdU IHC in P53 gene-edited mice treated with vehicle or 1,2-PD 3.5 days after 14 Gy TBI. Scale bar: 200 μ m. (C) Quantification of proliferating crypts in each group. A crypt containing more than 5 BrdU+ cells is recognized as a proliferating crypt. Values are represented by the *mean* \pm *SEM*; N =3 mice in each group, **P* <0.05, ***P* <0.01.

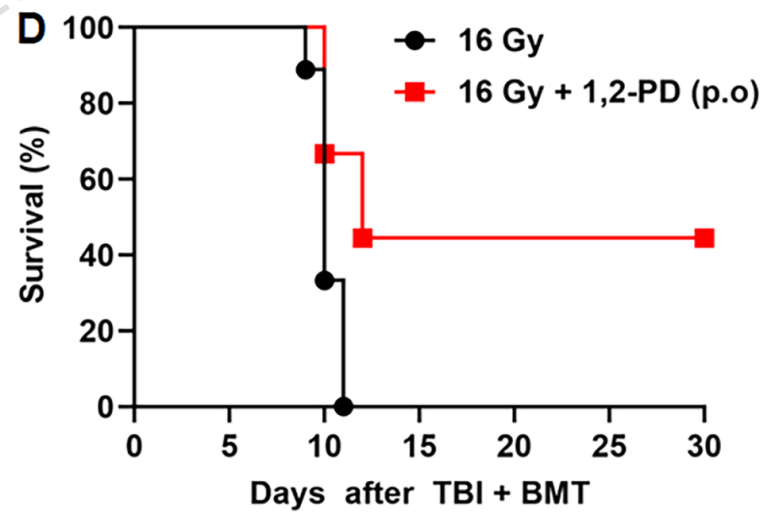
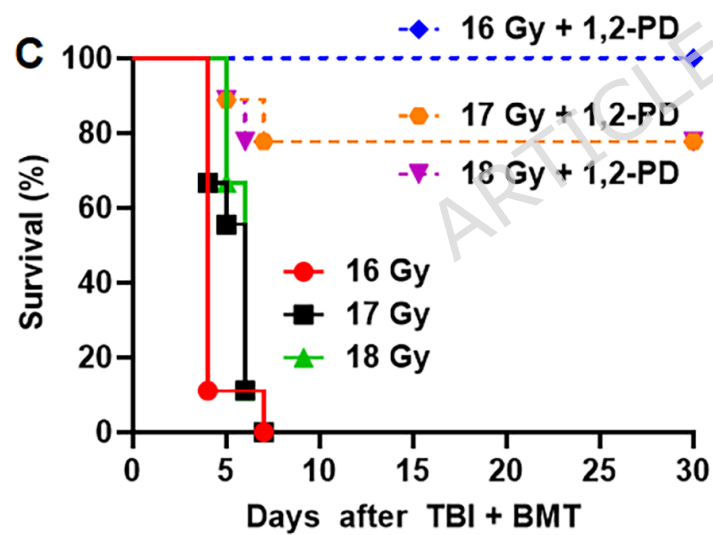
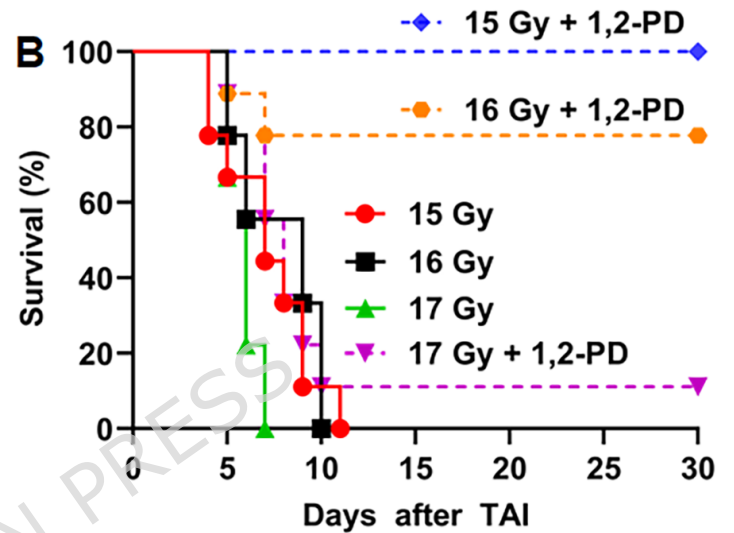
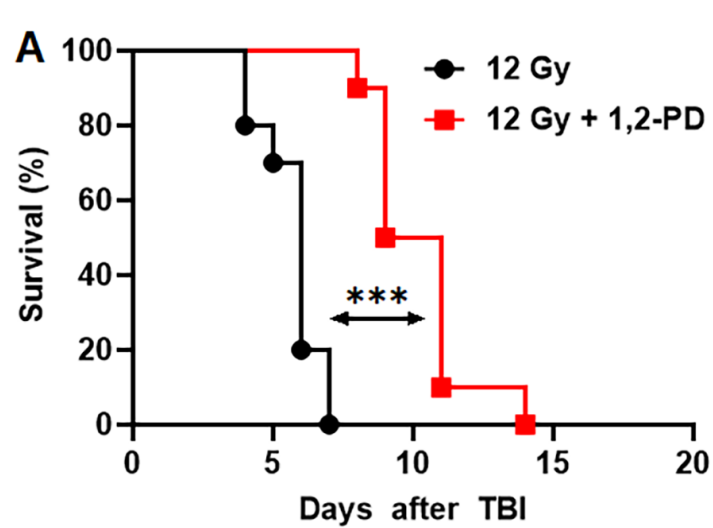
Figure 8. 1,2-PD Modulates Gene Expression Related to Cell Cycle and Hypoxia Response

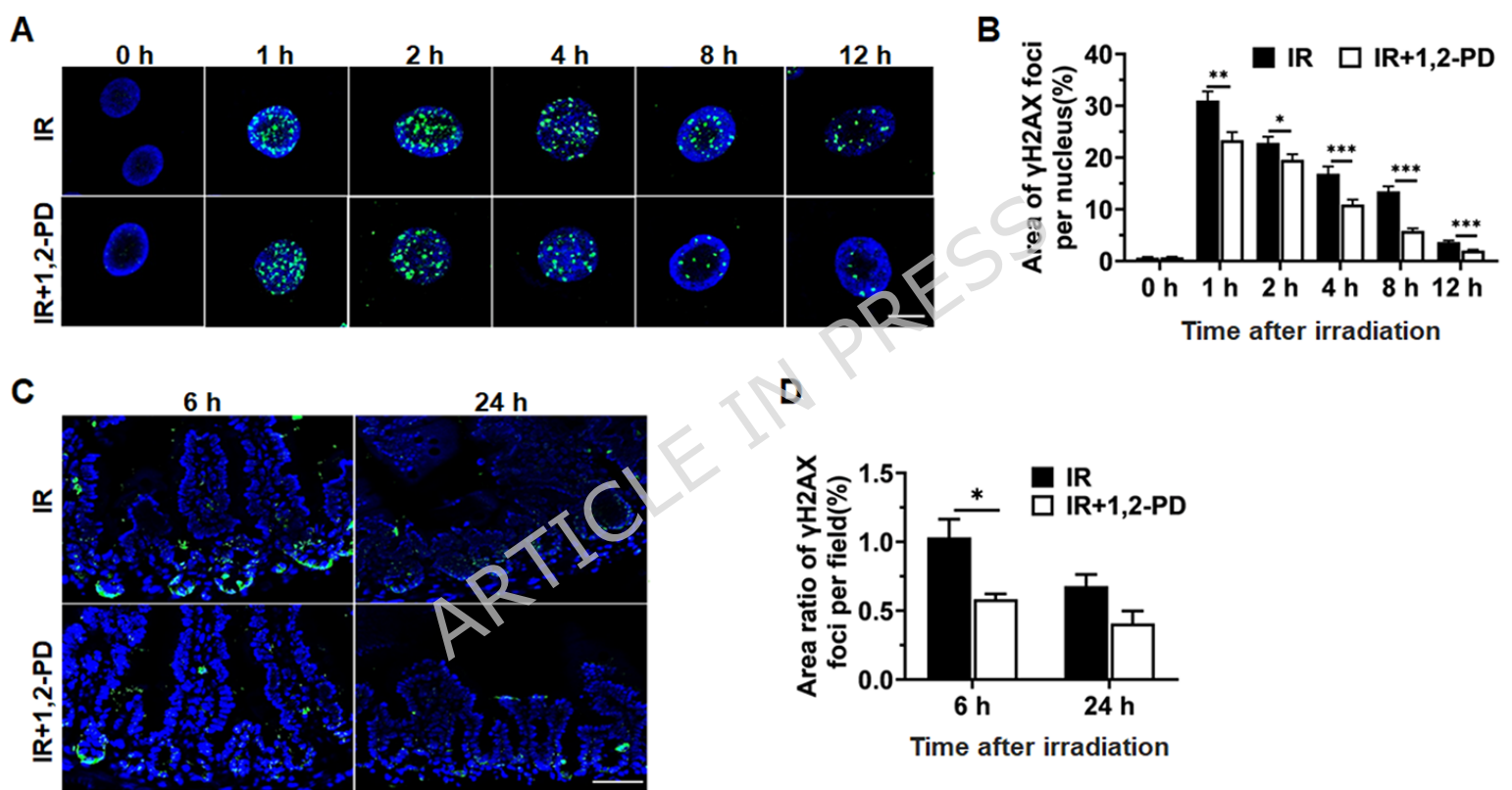
(A) RNA sequencing heatmap reveals that following a single intraperitoneal administration of 6 g kg⁻¹ 1,2-PD (PPG) 3 hours prior to irradiation, hypoxia response genes (Hif-2 α , Hif-3 α) and lipid metabolism/ antioxidant genes (Ppara α and ACOX2) were significantly upregulated, whilst G1/S transition drivers E2f3 and Cyclin D2 were markedly downregulated (n = 3).

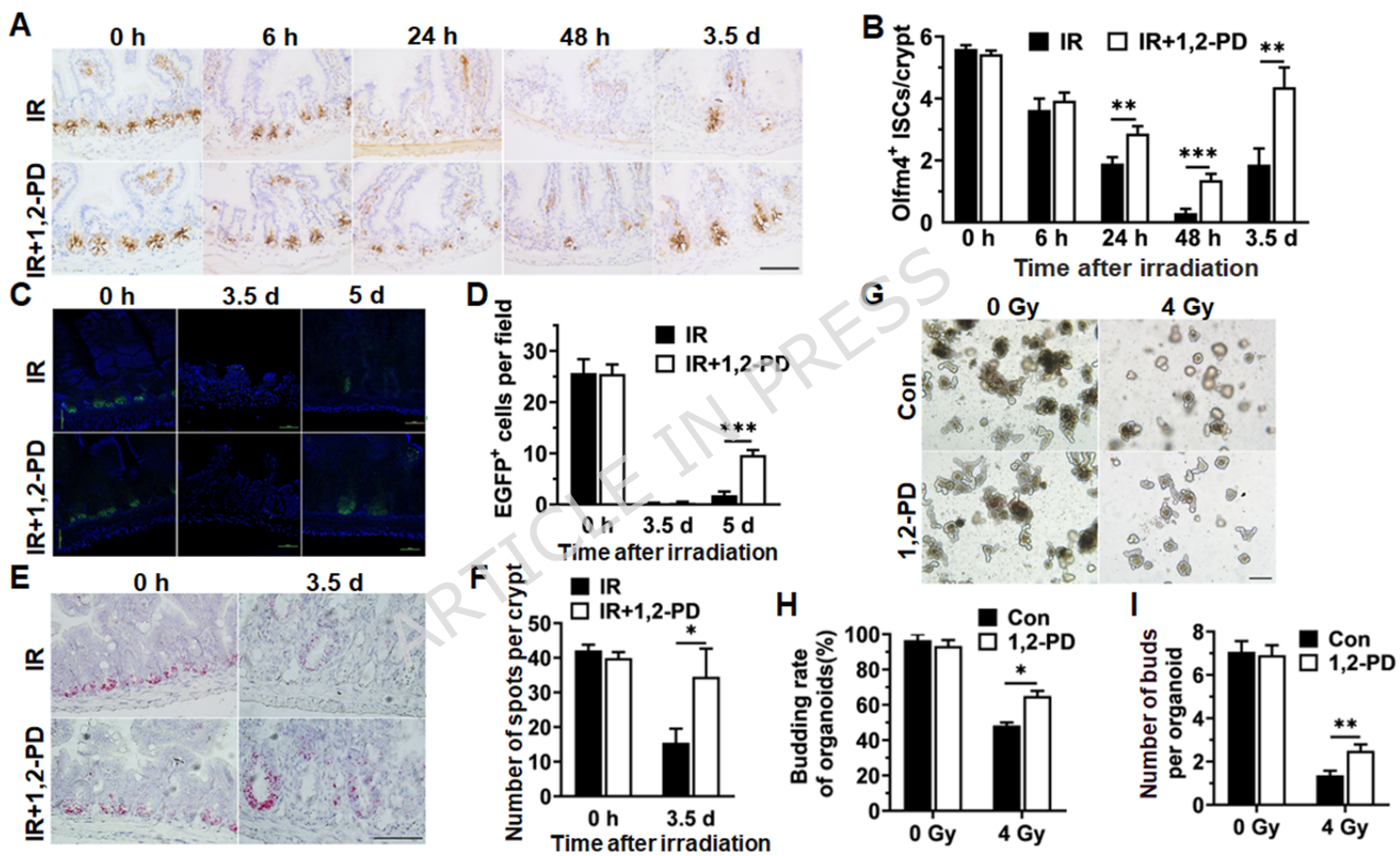
(B) RT-PCR validation: Compared to controls, 1,2-PD treatment increased

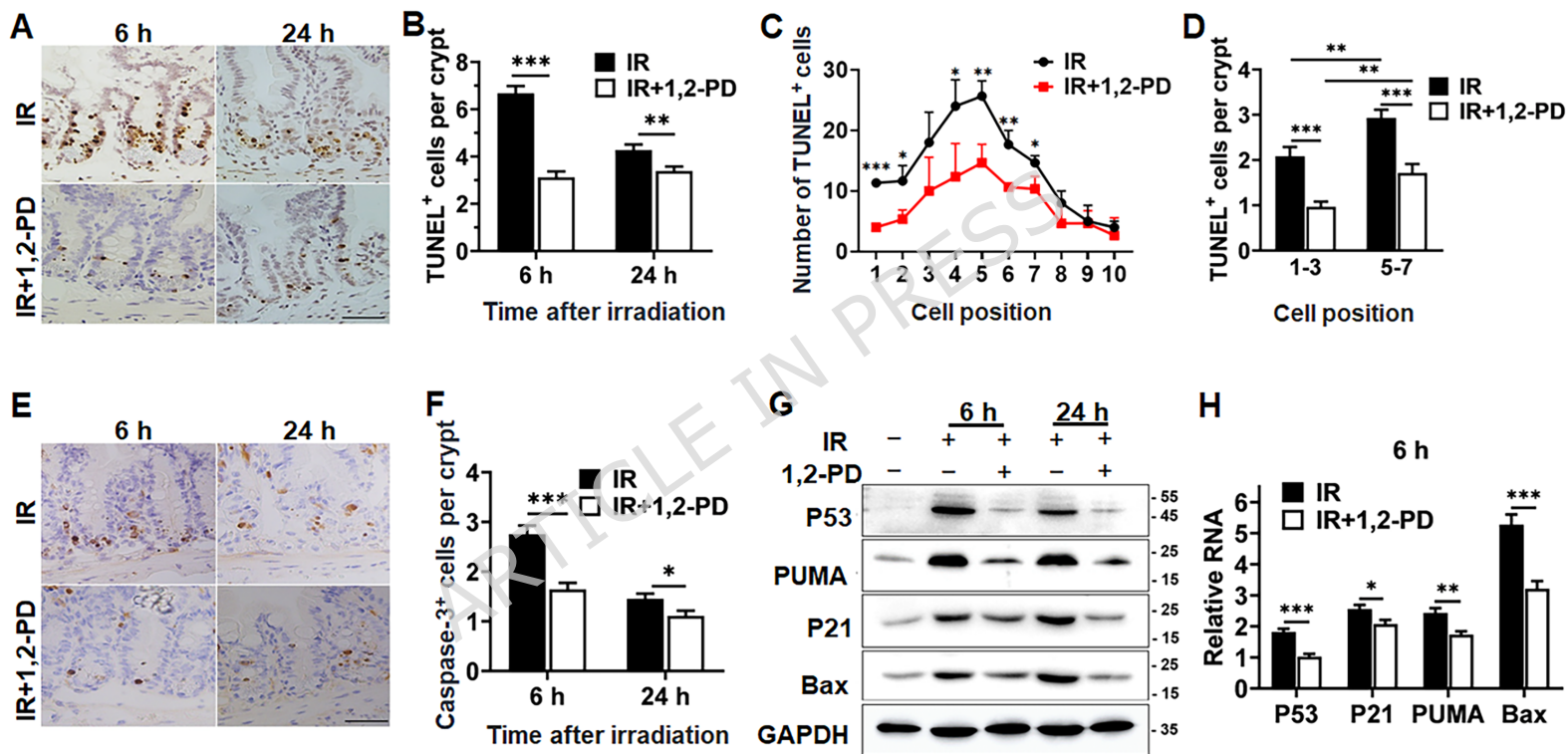
Hif-3a and Ppara α mRNA levels approximately twofold, while E2f3 and Ccnd2 decreased by approximately 50% (mean \pm SEM, n = 3, P < 0.01). These findings suggest that 1,2-PD may enhance intestinal radiation resistance by inducing hypoxic adaptation and inhibiting cell cycle progression. *P < 0.05, **P < 0.01, ***P < 0.001, **** P < 0.0001.

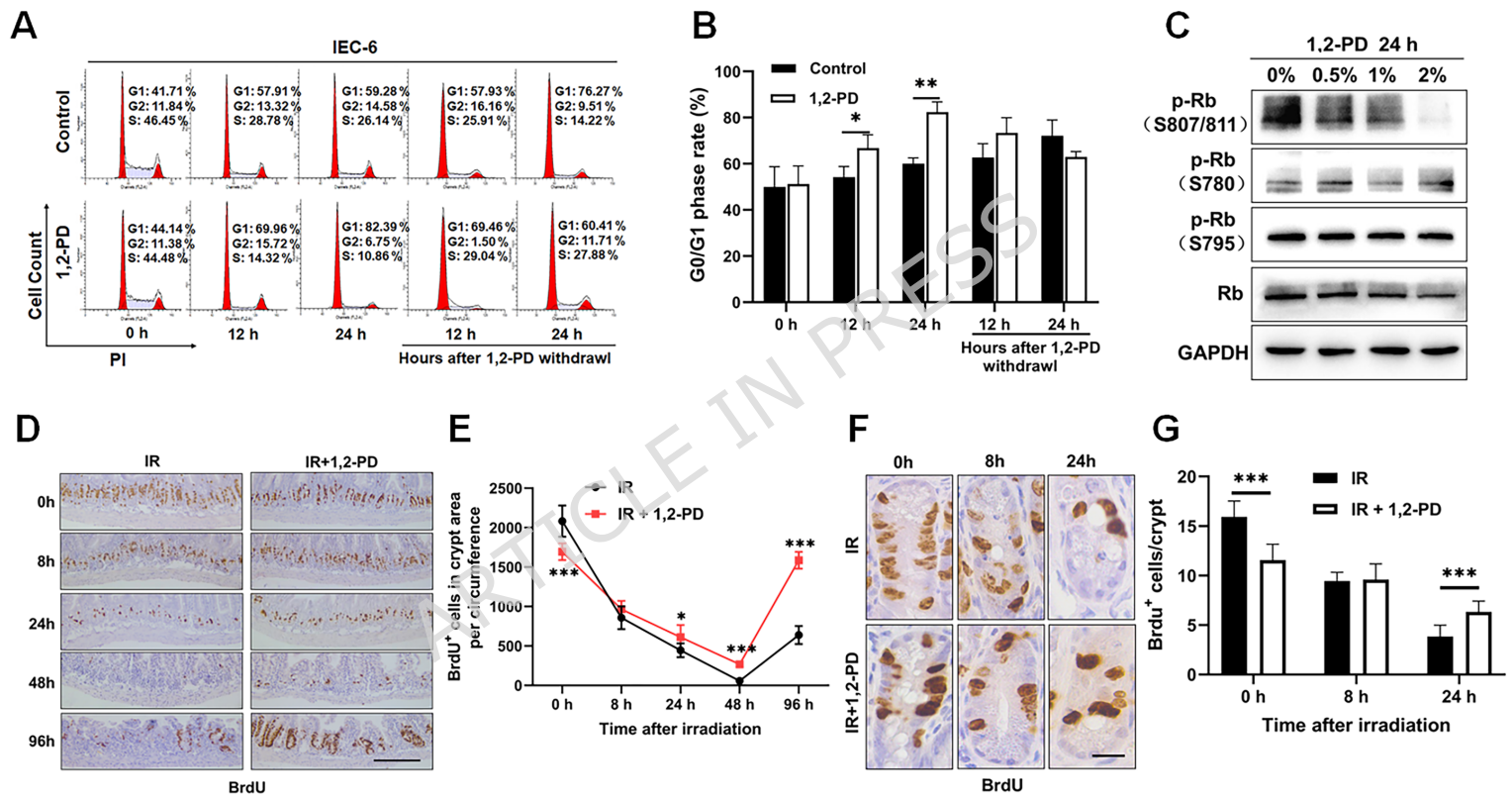
ARTICLE IN PRESS

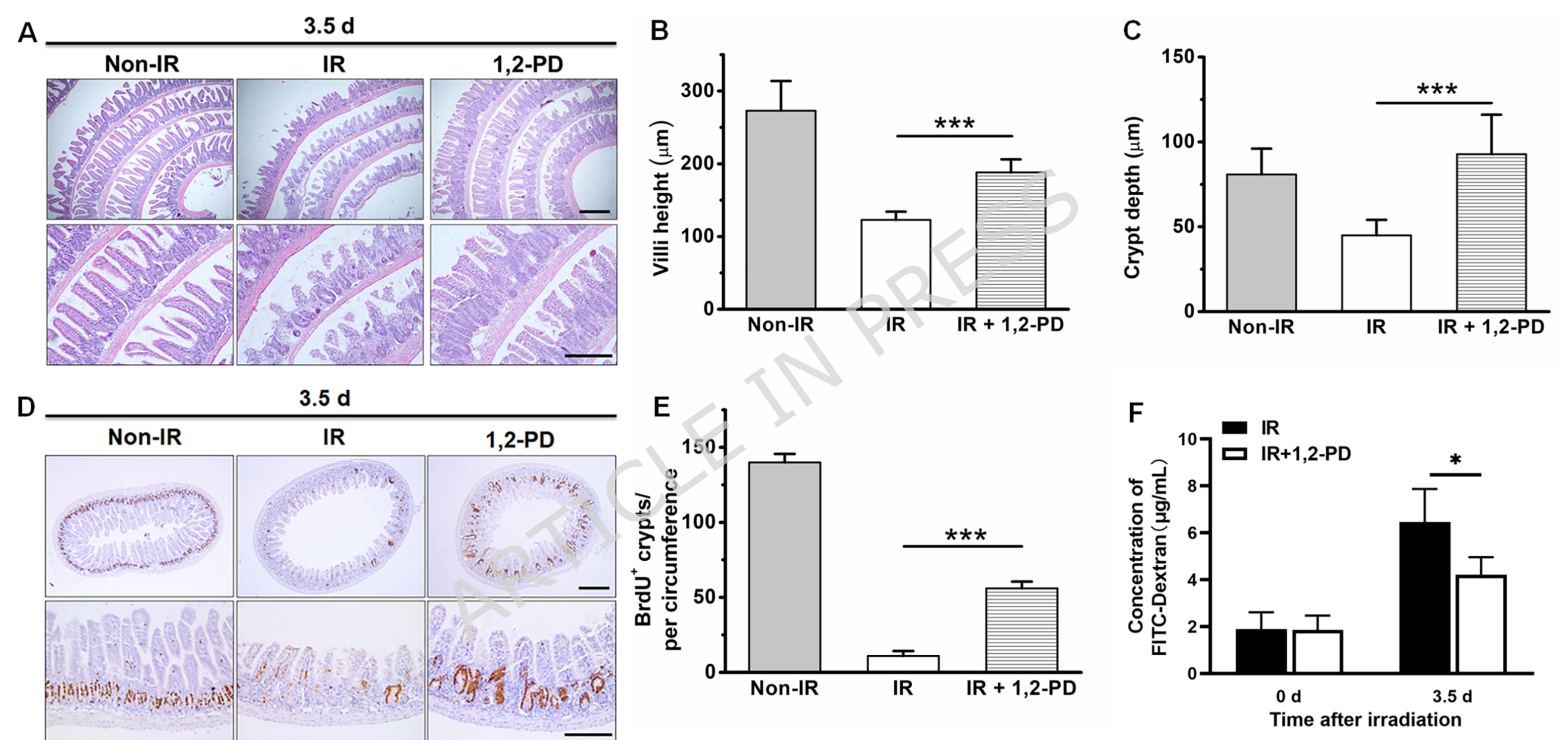


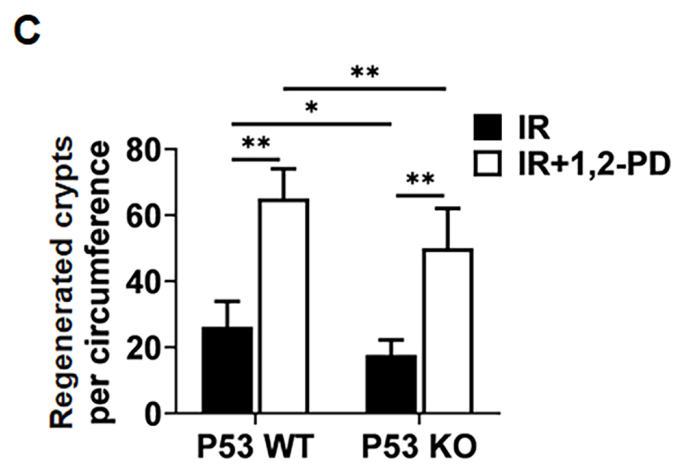
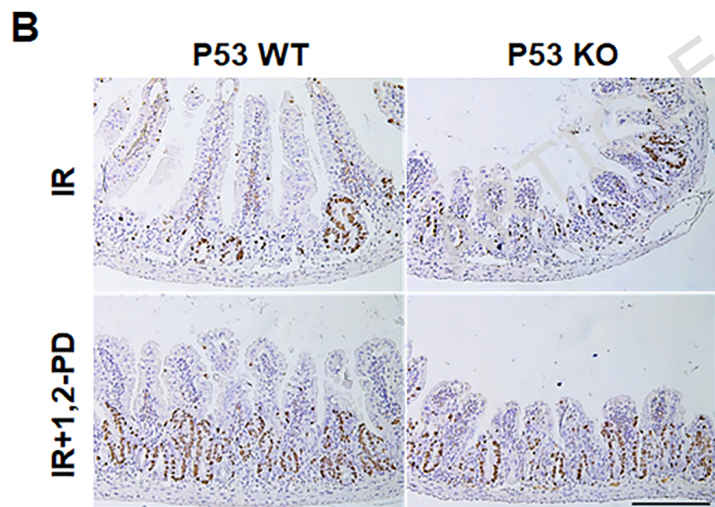
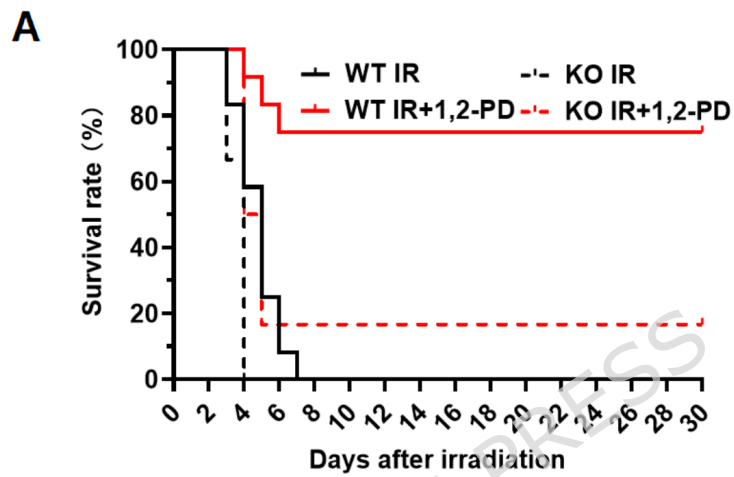


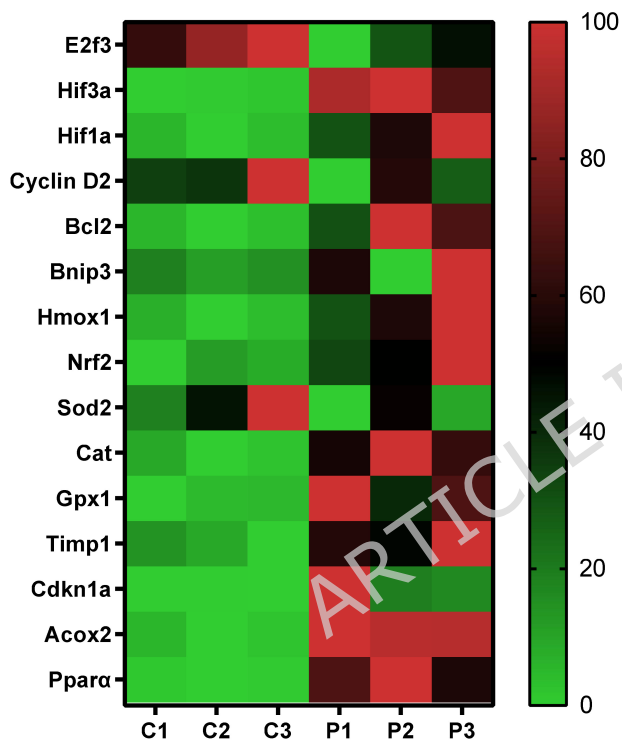










A**B**